

Numerical Analysis on Shimmying Wheels with Dry Friction Damper

Hanna Zsofia Horvath^{1*}, Denes Takacs²

¹ Department of Applied Mechanics, Faculty of Mechanical Engineering, Budapest University of Technology and Economics, H-1111 Budapest, Műegyetem rkp. 3, Hungary

² ELKH-BME Dynamics of Machines Research Group, H-1111 Budapest, Műegyetem rkp. 3, Hungary

* Corresponding author, e-mail: hanna.horvath@mm.bme.hu

Received: 26 August 2022, Accepted: 12 December 2022, Published online: 01 February 2023

Abstract

The dynamics of the 1.5-degree-of-freedom model of towed wheel is investigated. Dry friction at the king pin is considered, leading to a non-smooth dynamical system. Beyond analytical and numerical linear stability analysis, the nonlinear vibrations are investigated by numerical bifurcation analysis with smoothing and by numerical simulations with event handling. The effect of dry friction at the king pin on the birth of separated periodic branches is presented on bifurcation diagrams. The presence of bistable parameter domains is also shown. The effect of smoothing is investigated by comparing bifurcation diagrams of the smoothed and the original non-smooth systems.

Keywords

wheel shimmy, dry friction damper, non-smooth system, bifurcation analysis, numerical simulation, event handling

1 Introduction

Wheel shimmy, the lateral vibration of towed wheels [1–9] is under investigation in this study. This interesting phenomenon may cause serious accidents of motorcycles [10–11], trailers [12–15], articulated buses, airplane landing nose gears [16], shopping trolleys and even baby strollers.

Even though the shimmy phenomenon has been widely investigated in several studies, it has not been fully explored yet. One of the reasons is that the system of towed wheels is a complex dynamical system. The other reason is originated in the complicated nature of the wheel-ground contact. In this study, a single contact point model is used with a rigid caster, a rigid wheel and a laterally elastic king pin. Studies show that having dampers is an effective technique to avoid wheel shimmy; however, dry friction at the king pin was not investigated in the literature yet. Therefore, in this study we aim to analyze the effect of the non-smooth nature of dry friction.

The rest of the paper is organized as follows. In Section 2, the mechanical model of the towed wheel is introduced together with the governing equations derived by the basic law of dynamics. In Section 3, analytical and numerical results of the linear stability analysis are presented. The non-linear analysis is performed and the effect of dry friction

is shown in Section 4, using numerical bifurcation analysis and numerical simulations. Numerical results and the effect of smoothing are presented in Section 5. We summarize our results and give conclusions in Section 6.

2 Mechanical model and governing equations

The mechanical model of the towed wheel is shown in Fig. 1. The model consists of a rigid wheel with a single contact point connected to a rigid caster with caster length l . The system is towed with constant velocity V in the X direction in the horizontal (X, Y) plane. The mass and the rotation of the wheel is not taken into account, i.e., the rolling wheel is considered as a mass-less skate. It can be shown, that the kinematic constraint for the center point of the wheel is the same as for the rigid rolling wheel [17].

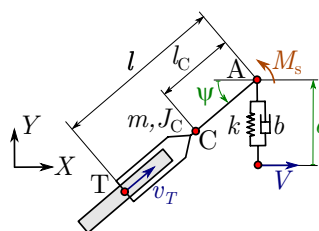


Fig. 1 The mechanical model of shimmying wheel

The overall mass of the system is m , the mass moment of inertia for the center of gravity C with respect to the axis of rotation Z is denoted by J_C . The distance between the king pin A and point C is l_C . The king pin is supported by a lateral spring with stiffness k and a lateral damping with damping factor b . Dry friction is also considered in the bearings of the king pin with the resultant torque M_s .

Since the speed of the king pin in the X direction is prescribed, a geometric constraint manifests in the following equation:

$$X_A = Vt + X_0, \quad (1)$$

where X_A is the X coordinate of the king pin and X_0 relates to the initial state.

To describe the motion of the system, one can use the yaw angle ψ and the lateral position of the king pin q as generalized coordinates. As mentioned before, in our study we do not take into account the rotation of the wheel about its rotational axis, which would be a so-called cyclic coordinate of the system when the pure rolling of the wheel is considered.

According to the kinematic constraint of pure rolling, the velocity of the center point of the wheel T is parallel to the caster, i.e.

$$\mathbf{v}_T = \begin{bmatrix} v_T \cos \psi \\ v_T \sin \psi \\ 0 \end{bmatrix} \quad (2)$$

By means of a transport formula, this velocity can be calculated as:

$$\begin{aligned} \mathbf{v}_T &= \mathbf{v}_A + \boldsymbol{\omega} \times \mathbf{r}_{AT} \\ &= \begin{bmatrix} V \\ \dot{q} \\ 0 \end{bmatrix} + \begin{bmatrix} 0 \\ 0 \\ \dot{\psi} \end{bmatrix} \times \begin{bmatrix} -l \cos \psi \\ -l \sin \psi \\ 0 \end{bmatrix} = \begin{bmatrix} V + l \sin \psi \dot{\psi} \\ \dot{q} - l \cos \psi \dot{\psi} \\ 0 \end{bmatrix}, \end{aligned} \quad (3)$$

where \mathbf{v}_A is the velocity of point A, $\boldsymbol{\omega}$ is the angular velocity of the caster and \mathbf{r}_{AT} is the position vector from point A to point T. Based on Eqs. (2) and (3):

$$v_T \cos \psi = V + l \sin \psi \dot{\psi}, \quad (4)$$

$$v_T \sin \psi = \dot{q} - l \cos \psi \dot{\psi}. \quad (5)$$

By performing algebraic manipulations with Eqs. (4) and (5), the velocity of point T can be calculated as:

$$v_T = V \cos \psi + \dot{q} \sin \psi, \quad (6)$$

and the kinematic constraint of pure rolling can be formulated as:

$$\dot{q} = \frac{l}{\cos \psi} \dot{\psi} + V \tan \psi. \quad (7)$$

The free body diagram of the wheel-caster system, modelled as a mass-less skate, can be seen in Fig. 2. The lateral spring force can be calculated as $F_s = kq$, the lateral damping force as $F_d = b\dot{q}$. The dry friction at the king pin is taken into account with the non-smooth nature of torque $M_s = -M_0 \operatorname{sgn} \dot{\psi}$. Note that a more complex friction model could also be investigated instead of this simple Coulomb-friction law. Since the aim of this study is to gain basic knowledge about the non-smooth nature of dry friction at the king pin of shimmying wheels, this assumption is reasonable. The study can be later expanded with more complex friction laws.

The equations of motion can be derived by using the basic law of dynamics:

$$ma_{cX} = F_A - F_T \sin \psi, \quad (8)$$

$$ma_{cY} = -F_s - F_d + F_T \cos \psi, \quad (9)$$

$$\begin{aligned} J_C \ddot{\psi} &= -F_T (l - l_C) - F_s l_C \cos \psi \\ &\quad - F_d l_C \cos \psi - F_A l_C \sin \psi + M_s. \end{aligned} \quad (10)$$

From Eq. (9), the constraining force at point T can be expressed as:

$$F_T = \frac{ma_{cY} + F_s + F_d}{\cos \psi} = \frac{ma_{cY} + kq + b\dot{q}}{\cos \psi}, \quad (11)$$

from Eq. (8), the longitudinal constraining force at the king pin is:

$$\begin{aligned} F_A &= ma_{cX} + F_T \sin \psi \\ &= ma_{cX} + (ma_{cY} + kq + b\dot{q}) \tan \psi. \end{aligned} \quad (12)$$

The velocity of the center of gravity can be calculated as:

$$\begin{aligned} \mathbf{v}_C &= \mathbf{v}_A + \boldsymbol{\omega} \times \mathbf{r}_{AC} \\ &= \begin{bmatrix} V \\ \dot{q} \\ 0 \end{bmatrix} + \begin{bmatrix} 0 \\ 0 \\ \dot{\psi} \end{bmatrix} \times \begin{bmatrix} -l_C \cos \psi \\ -l_C \sin \psi \\ 0 \end{bmatrix} = \begin{bmatrix} V + l_C \sin \psi \dot{\psi} \\ \dot{q} - l_C \cos \psi \dot{\psi} \\ 0 \end{bmatrix}. \end{aligned} \quad (13)$$

Thus, the acceleration of point C is:

$$\begin{aligned} \mathbf{a}_C &= \begin{bmatrix} a_{cX} \\ a_{cY} \\ 0 \end{bmatrix} = \dot{\mathbf{v}}_C \\ &= \begin{bmatrix} l_C \cos \psi \dot{\psi}^2 + l_C \sin \psi \ddot{\psi} \\ \ddot{q} + l_C \sin \psi \dot{\psi}^2 - l_C \cos \psi \ddot{\psi} \\ 0 \end{bmatrix}. \end{aligned} \quad (14)$$

Substituting the above calculated accelerations and forces into Eq. (10) leads to the following second-order differential equation:

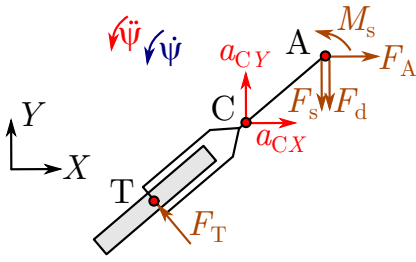


Fig. 2 The free body diagram of the mechanical system

$$\begin{aligned}
 & (J_C + ml_C^2 - mll_C)\ddot{\psi} + mll_C \tan\psi\dot{\psi}^2 \\
 & + \left(m \frac{l}{\cos\psi} - ml_C \cos\psi \right) \ddot{q} + b \frac{l}{\cos\psi} \dot{q} \\
 & + k \frac{l}{\cos\psi} q - M_s = 0.
 \end{aligned} \tag{15}$$

The first and second derivatives of the lateral position q can be expressed with ψ , Ω and $\dot{\Omega}$, i.e. $\dot{q} = \dot{q}(\psi, \Omega)$ and

$$\begin{aligned}
 \dot{\Omega} = & - \frac{m \frac{l^2 \sin\psi}{\cos^3\psi}}{J_C + ml_C^2 - 2mll_C + m \frac{l^2}{\cos^2\psi}} \Omega^2 - \frac{m \frac{l}{\cos^3\psi} V - m \frac{l_C}{\cos\psi} V + b \frac{l^2}{\cos^2\psi}}{J_C + ml_C^2 - 2mll_C + m \frac{l^2}{\cos^2\psi}} \Omega - \frac{k \frac{l}{\cos\psi}}{J_C + ml_C^2 - 2mll_C + m \frac{l^2}{\cos^2\psi}} q \\
 & - \frac{b \frac{l \sin\psi}{\cos^2\psi} V}{J_C + ml_C^2 - 2mll_C + m \frac{l^2}{\cos^2\psi}} + \frac{M_s}{J_C + ml_C^2 - 2mll_C + m \frac{l^2}{\cos^2\psi}}.
 \end{aligned} \tag{19}$$

Since the system of equations of motion (Eqs. (17–19)) consists of three first-order differential equations, the state space is three-dimensional and thus, the mechanical model has 1.5 DoF. The vector of state variables is:

$$\mathbf{x} = [\psi \quad q \quad \Omega]^T. \tag{20}$$

3 Linear stability analysis

For linear stability analysis of the rectilinear motion, the equations of motion are linearized around the trivial solution $\mathbf{x}(t) \equiv \mathbf{0}$. The linearized governing equations for the dry friction-free case ($M_0 = 0$) can be written as:

$$\dot{\mathbf{x}} = \mathbf{A}\mathbf{x}, \tag{21}$$

with coefficient matrix:

$$\mathbf{A} = \begin{bmatrix} 0 & 0 & 1 \\ V & 0 & l \\ -\frac{b l V}{J_T} & -\frac{k l}{J_T} & -\frac{m(l-l_C)V + b l^2}{J_T} \end{bmatrix}, \tag{22}$$

$\ddot{q} = \ddot{q}(\psi, \Omega, \dot{\Omega})$ therefore \ddot{q} is not a state variable anymore. By substituting \dot{q} and \ddot{q} into Eq. (15), we obtain:

$$\begin{aligned}
 & \left(J_C + ml_C^2 - 2mll_C + m \frac{l^2}{\cos^2\psi} \right) \ddot{\psi} + m \frac{l^2 \sin\psi}{\cos^3\psi} \dot{\psi}^2 \\
 & + \left(m \frac{l}{\cos^3\psi} V - m \frac{l_C}{\cos\psi} V + b \frac{l^2}{\cos^2\psi} \right) \dot{\psi} \\
 & + k \frac{l}{\cos\psi} q + b \frac{l \sin\psi}{\cos^2\psi} V - M_s = 0.
 \end{aligned} \tag{16}$$

This together with Eq. (7) provide the governing equations of our system. Thanks to the considered frictional torque at the king pin, the mathematical model of the system is non-smooth for $M_0 \neq 0$. We introduce and rewrite the governing equations into a system of first order differential equations (Eqs. (17)–(19)):

$$\dot{\psi} = \Omega, \tag{17}$$

$$\dot{q} = \frac{l}{\cos\psi} \Omega + V \tan\psi, \tag{18}$$

where the mass moment of inertia for the center point of the wheel T with respect to the axis of rotation Z is:

$$J_T = J_C + m(l-l_C)^2. \tag{23}$$

Using the exponential trial solution of the system, the characteristic equation can be obtained as:

$$\lambda^3 + \underbrace{\frac{m(l-l_C)V + b l^2}{J_T}}_{=a_1} \lambda^2 + \underbrace{\frac{b l V + k l^2}{J_T}}_{=a_2} \lambda + V \underbrace{\frac{k l}{J_T}}_{=a_3} = 0. \tag{24}$$

The linear stability can be investigated by the Routh-Hurwitz criteria [18]. The so-called Routh-Hurwitz matrix has the form:

$$\mathbf{H} = \begin{bmatrix} a_1 & 1 & 0 \\ a_3 & a_2 & a_1 \\ 0 & 0 & a_3 \end{bmatrix}. \tag{25}$$

The rectilinear motion is linearly stable if each principal minor of the Routh-Hurwitz matrix is positive:

$$H_1 = a_1 > 0, \quad (26)$$

$$H_2 = a_1 a_2 - a_3 > 0, \quad (27)$$

$$H_3 = H_2 a_3 > 0. \quad (28)$$

Unfortunately, no closed-form formula can be calculated for the damped case. However, if the lateral damping is neglected, namely $b = 0$, the stability criteria can be simplified to the following three conditions: $l > l_c$, $l > (J_c + ml_c^2)/(ml_c)$ and $l > 0$. All in all, the strictest criterion means that the rectilinear motion is linearly stable if the caster length is larger than the critical value l^{crit} , namely:

$$l > l^{\text{crit}} = \frac{J_c + ml_c^2}{ml_c}. \quad (29)$$

Note that for this undamped case, the critical caster length does not depend on the towing speed, which is against our physical sense.

On the other hand, linear stability can be analyzed numerically in the damped case too. The critical caster length for the damped case is shown for different towing speeds in the stability chart of Fig. 3 together with the analytical result of the undamped case. The parameter values of the system are summarized in Table 1.

In the linear stability chart of Fig. 3, the light gray and the white areas correspond to the linearly unstable and stable rectilinear motions for the undamped case, respectively. The dark gray area corresponds to the linearly unstable rectilinear motion for the damped case.

As can be seen in Fig. 3, the rectilinear motion is stable for all towing speeds if the caster length is slightly above

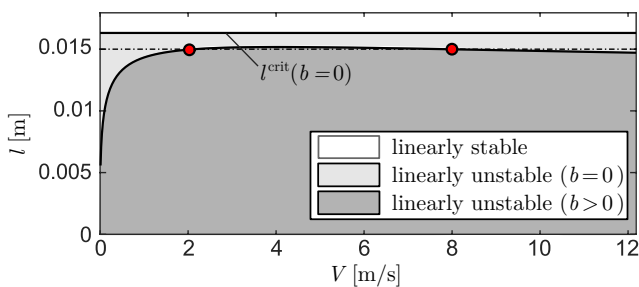


Fig. 3 Linear stability chart for the undamped and the damped cases

Table 1 Parameter values of the system

Notation, unit	Parameter value
m [kg]	0.0672
l [m]	0.015
l_c [m]	0.012
J_c [kg m ²]	3.48×10^{-6}
k [N/m]	1000
b [Ns/m]	0.5

0.015 m. For the investigated caster length $l = 0.015$ m (indicated by the horizontal black dashed line), the rectilinear motion is unstable approximately between 2.14 m/s and 7.83 m/s, see the stability boundaries (i.e., the Hopf bifurcation points) plotted with red dots.

4 Nonlinear analyses

In nonlinear systems, some phenomena may be undiscovered if only linear stability analysis is performed. Due to the complexity of the non-smooth nature originated in dry friction, the nonlinear analysis of the shimmying wheel needs special attention. As a first step, the non-smooth nature is omitted by using a smoothing function, and we perform numerical bifurcation analysis with a *Matlab* package called *DDE Biftool* [19], which tracks the periodic solutions with collocation, using the pseudo-arclength method. As a second technique, we do numerical simulations with event detection to handle the non-smoothness of the original system and verify the results.

Based on the characteristics of the dry friction ($M_s = -M_0 \text{sgn} \Omega$), there is a qualitative change in the dynamics when $\Omega = 0$. Hence, it is the switching surface of the non-smooth system.

4.1 Numerical bifurcation analysis with smoothing

To handle the non-smooth characteristic of the friction torque M_s , a smoothed step-function can be formulated as:

$$H(\Omega) = \tanh\left(\frac{\Omega}{\epsilon}\right), \quad (30)$$

with smoothing parameter ϵ . The smoothness depends on the smoothing parameter, i.e., the smaller the value of ϵ is, the more sudden the switching is. Using the above mentioned function, the torque originated from dry friction is considered as:

$$M_s = -M_0 H(\Omega). \quad (31)$$

By implementing the governing equations into *Matlab*, numerical bifurcation analysis is performed with the help of *DDE Biftool* [19]. Namely, Hopf bifurcations at the linear stability boundaries are located and the emerging periodic solutions are followed using continuation.

Bifurcation diagrams for the amplitude Ω_{max} of the yaw rate are plotted versus the towing speed V , see Fig. 4. In the bifurcation diagrams, the stable and the unstable rectilinear motion are marked with thin solid blue and dashed red lines, respectively. The stable and the unstable branches of periodic orbits are depicted with thick solid blue and thick dashed

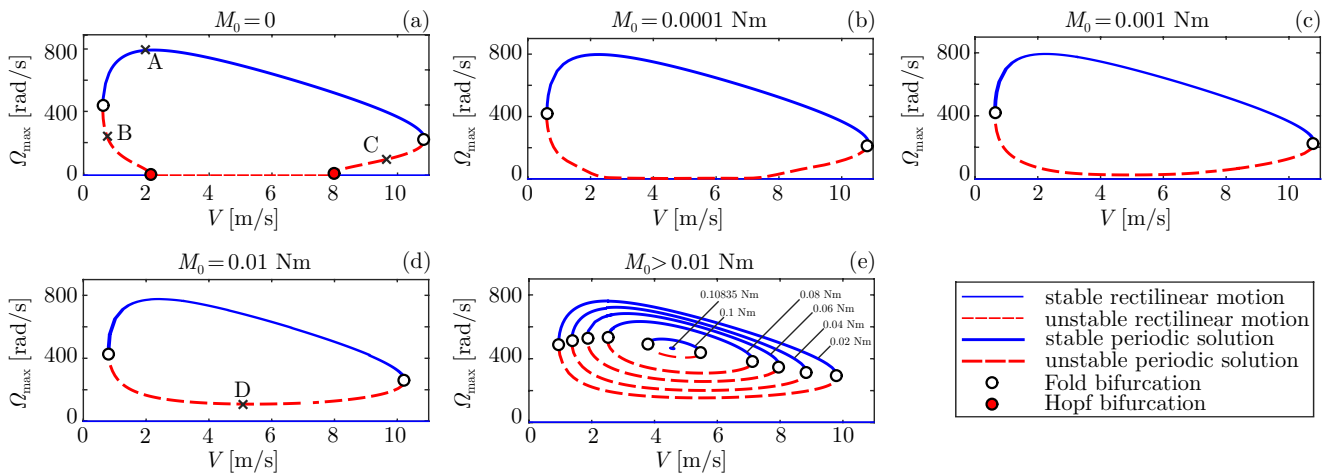


Fig. 4 Bifurcation diagrams for the amplitude Ω_{\max} of the yaw rate for different dry friction values: (a) $M_0 = 0$; (b) $M_0 = 0.0001$ Nm; (c) $M_0 = 0.001$ Nm; (d) $M_0 = 0.01$ Nm; (e) $M_0 > 0.01$ Nm

red curves, respectively. Fold bifurcations of periodic orbits are marked by white circles, while red circles refer to Hopf bifurcations at the linear stability boundaries. Some parameter points are also plotted for which the time histories of periodic motions are shown in Section 5. Note that the bifurcation diagrams are only shown for the yaw rate, but they could be depicted for the other state variables, as well.

For the parameter setup specified in Table 1, the rectilinear motion is linearly unstable approximately between 2.14 m/s and 7.83 m/s, see panel (a) of Fig. 4. This agrees with the result of the linear stability analysis described in Section 3. At the linear stability boundaries, the Hopf bifurcations are subcritical, that is, unstable periodic orbits emerge from the Hopf-points. Unsafe bistable parameter ranges can be also seen, where stable stationary rolling and large amplitude stable oscillations coexist. This means that for small perturbations, the oscillations decay but for large enough perturbations large amplitude vibrations occur.

In the presence of dry friction (namely for $M_0 > 0$), a so-called isola is born, i.e., a separated periodic branch can be discovered over the stable rectilinear domain, see panels (b)–(e) of Fig. 4. This means that the stationary rolling is stable for all towing speeds, but shimmy motion may still occur. The importance of nonlinear analysis is justified by the fact that the existence of such isolas cannot be shown with linear analysis.

The greater the value of M_0 is, the smaller the size of the isola is, see panel (e) of Fig. 4. Consequently, the domain of attraction of the rectilinear motion is also larger. For the investigated parameter values, the isola vanishes when $M_0 = 0.10835$ Nm, and the rectilinear motion becomes the only stable solution within the state space.

4.2 Numerical simulations with the non-smooth nature of the system taken into account

For the numerical simulations, the *ODE45 Matlab* routine was used with initial conditions:

$$\mathbf{x}(t = 0) = [0 \quad 0 \quad \Omega_0]^T, \quad (32)$$

which refer to an impact-like perturbation of the system. This initial condition is chosen due to the fact that it can be easily realized in experiments. The simulations are run for 50 different initial yaw rate values (namely, $1 \text{ rad/s} < \Omega_0 < 1000 \text{ rad/s}$) and for 50 different towing speed V values (namely, $0 \text{ m/s} < V < 12 \text{ m/s}$). In case of $M_0 > 0$, the non-smooth nature of the system is taken into account by event handling. Namely, the sign of the yaw rate Ω is investigated and two kind of events are detected: when Ω becomes positive and when Ω becomes negative.

Since for parameter values described in Table 1, the transient vibrations die out typically in 5 s, a maximum simulation time of 10 s is set for each simulation. In addition, if the tendency in the time histories of the yaw angle or the yaw rate clearly shows where the solution is converging, the simulation is stopped in order not to waste computational time for simple cases. To detect the events with a larger precision, a tolerance $\Omega_{\text{tol}} = 10^{-2} \text{ rad/s}$ is used, and the time step of the simulation is reduced close to the switching surface $\Omega = 0$ until the achieved tolerance is reached. At the end of each simulation, the maximum amplitude of the yaw rate is determined based on the time graphs. Namely, if the solution converges to the large amplitude vibrations, the amplitude of the last couple of periods of the solution is read out. If the solution converges to the stable rectilinear motion, zero amplitude

is noted. On the 50×50 mesh of the towing speed and the initial yaw rate, the boundary between the domain of attraction of the stable periodic solution and the domain of attraction of the rectilinear motion can be depicted.

The results of the numerical simulations can be seen in Fig. 5. For different amount of dry friction, the thick black curve shows the boundary between the domain of attraction of the stable periodic solution (see the gray areas) and the domain of attraction of the stable rectilinear motion (see the white areas). The amplitudes of the stable limit branches are marked with black pluses.

On the one hand, large amplitude oscillations may appear even for small perturbations for $M_0 > 0$, see panels (b)–(e) of Fig. 5. On the other hand, dry friction helps in a way that the domain of attraction of the stable rectilinear motion gets larger for larger values of M_0 . The gray area disappears abruptly at approximately $M_0 = 0.073$ Nm. Note that the numerical simulation results are only shown for the yaw rate, but they could be depicted for the other state variables, as well.

5 Results and comparison

In Fig. 6, the amplitudes of the stable limit cycles obtained by the numerical simulations and the boundary of the domain of attraction are plotted with black pluses and with a solid black curve, respectively. The stable and unstable branches of periodic orbits obtained by the numerical bifurcation analysis of the smoothed system are also shown with thick solid blue and thick dashed red curves, respectively. The two types of results differ significantly for higher towing speeds. Namely, the Fold point at approximately 11 m/s does not coincide with the point which separates the boundary of the domain of attraction and the stable limit cycle.

In Fig. 6, the results are depicted for the dry friction free case. Similar discrepancy can be observed here, hence, the difference may not be originated in the smoothing, but it is resulted by the fact that the initial condition used in the simulations may not be located on the center manifold of the nonlinear system. Namely, for $M_0 = 0$, the tangent of the center manifold [20] can be calculated based on the eigenvalues and the eigenvectors of the linearized system. The initial condition given by Eq. (32) does not fit to this tangent plane. The domains of attraction presented in Fig. 5 relate to a certain section of the state space while amplitudes in Fig. 4 correspond to the limit cycles belonging to the center manifold.

The numerical simulation and bifurcation analysis results are also compared for $M_0 = 0.01$ Nm, see Fig. 7. A qualitative agreement can be seen, i.e., a separated periodic branch

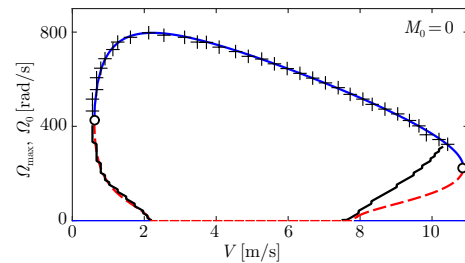


Fig. 6 Comparison of the numerical simulation and numerical bifurcation analysis results for $M_0 = 0$

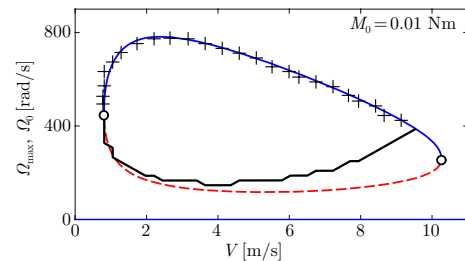


Fig. 7 Comparison of the numerical simulation and numerical bifurcation analysis results for $M_0 = 0.01$ Nm

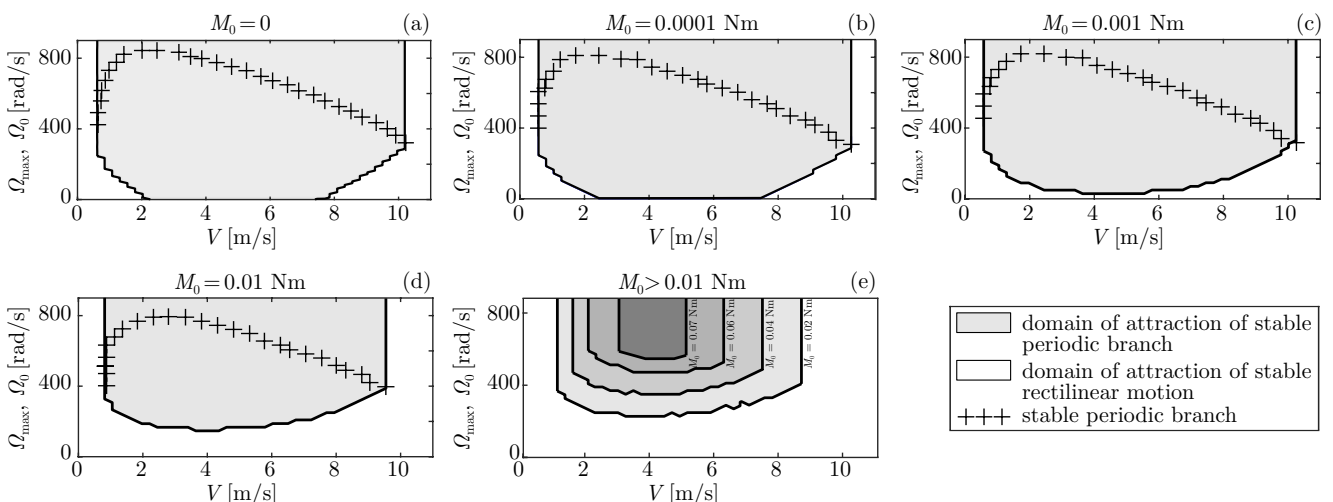


Fig. 5 The boundary between the domain of attraction of the stable periodic solution and the stable rectilinear motion for different dry friction values: (a) $M_0 = 0$; (b) $M_0 = 0.0001$ Nm; (c) $M_0 = 0.001$ Nm; (d) $M_0 = 0.01$ Nm; (e) $M_0 > 0.01$ Nm; black pluses refer to the amplitudes of the stable periodic branches

coexist with the stable rectilinear motion. As mentioned above, the unstable periodic orbit obtained by the bifurcation analysis differs significantly from the boundary of the domain of attraction shown with the black curve.

For parameters points A, B, C and D marked in Fig. 4, the stable and unstable oscillations of the yaw angle $\psi(t)$, the lateral displacement of the king pin $q(t)$ and the yaw rate $\Omega(t)$ are plotted versus time $t \in [0, T]$ with solid blue and solid red curves respectively, see Fig. 8. Here, T is the time period of the periodic solutions, namely $T = 1/f$ where f is the vibration frequency. The dry friction, the towing speed, the maximum values of the state variables and the vibration frequencies f for parameter points A, B, C and D are summarized in Table 2.

In case of $M_0 = 0.01$ Nm (see panel (D) in Fig. 8), we are not close to the switching manifold, i.e., the yaw rate Ω does not stay in the vicinity of zero. Therefore, these time graphs confirm that the difference in the results of the two methods are not originated in the smoothing.

In panel (a) of Fig. 9, the time graphs obtained by the two different methods are compared to each other for parameter point A. The stable oscillations obtained by the numerical simulations of the non-smooth system and the bifurcation analysis of the smoothed system are marked by solid blue curves and black stars, respectively. The two methods give qualitatively the same results, but

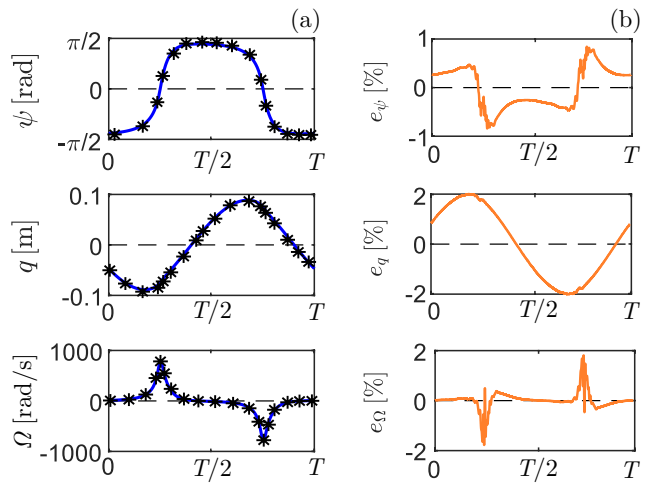


Fig. 9 Comparison of the numerical simulation and numerical bifurcation analysis results for $M_0 = 0$ Nm: (a) time graphs; (b) relative errors with respect to the limit cycle amplitude

some discrepancy can be observed, which may result from the numerical errors of the two methods. The relative errors are calculated based on the difference of the signals and the amplitude of the limit cycle. As can be seen in Fig. 9(b), they do not exceed 2%.

Note that the periodic motion has similar characteristics as in [5], but the vibration frequencies are somewhat larger. However, for the parameter setup in investigation, larger vibration frequencies can be feasible for the vibration amplitudes summarized in Table 2.

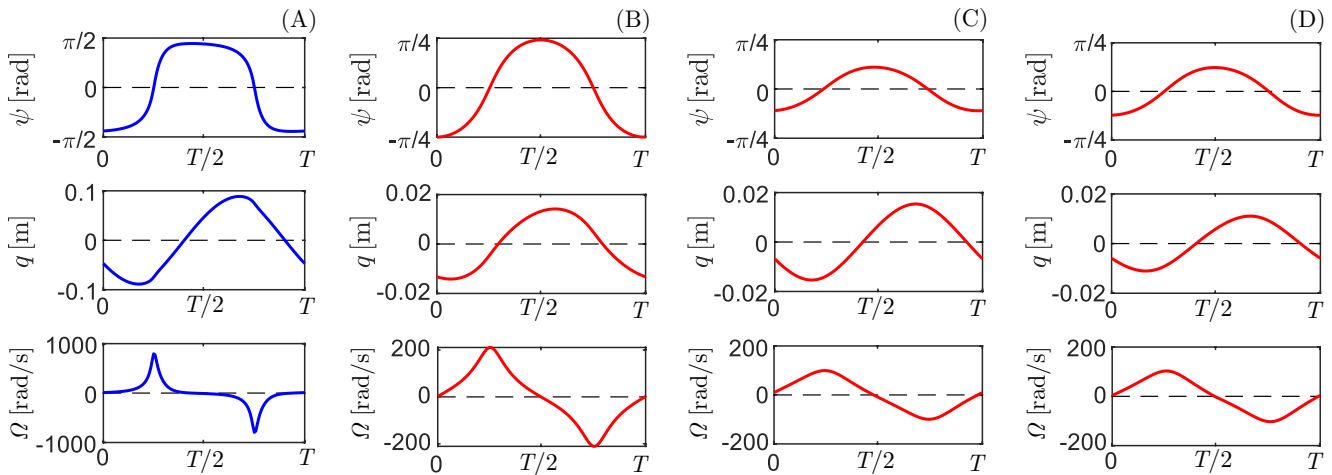


Fig. 8 The stable (blue) and the unstable (red) oscillations of the yaw angle $\psi(t)$, the lateral displacement of the king pin $q(t)$ and the yaw rate $\Omega(t)$ for parameter points (A), (B), (C) and (D)

Table 2 Results for the parameter points, obtained by the numerical bifurcation analysis of the smoothed system

#	M_0 [Nm]	V [m/s]	ψ_{\max} [rad]	q_{\max} [m]	Ω_{\max} [rad/s]	f [Hz]
A	0	2.0	1.39	0.089	795	22.8
B	0	0.8	0.79	0.014	211	28.9
C	0	9.7	0.35	0.015	100	40.0
D	0.01	5.1	0.39	0.011	103	36.9

One of the goals of this study was to analyze the effect of smoothing. On the one hand, the numerical bifurcation analysis with smoothing requires lower computational effort than the numerical simulations. On the other hand, the smoothing introduces a relatively large viscose damping to the system in the linear domain if $M_0 > 0$, which may modify the resulting periodic solutions to a notable extent. In addition, the bifurcation analysis results depend on the value of the smoothing parameter ϵ .

Unfortunately, the numerical simulation and the numerical bifurcation results cannot be compared to each other directly, since they are obtained in different sections of the state space. However, based on the time graphs of panel (a) of Fig. 9, it may be concluded that the numerical bifurcation analysis with smoothing provides acceptable results with respect to the numerical simulations.

6 Conclusions

In this study, the shimmy motion of a towed rigid wheel was investigated, taking dry friction at the king pin into account. The governing equations were derived from the basic law of dynamics. For the undamped case, the critical value of the caster length was calculated analytically. Linear stability boundaries were investigated numerically and summarized in a linear stability chart.

Nonlinear analysis was performed with two different methods: numerical bifurcation analysis with smoothing and numerical simulations taking the non-smooth nature into account by event handling. Bistable regions and isolated periodic solutions were discovered. Introducing dry friction at the king pin enlarges the domain of attraction of the stable rectilinear motion. It was also shown that the linearly undeterminable isolas vanish with higher values

of dry friction at the king pin. Although smoothing may introduce viscose damping into the system, it seems that the numerically affordable bifurcation analysis provides reasonable results. Hence, experiments with impact-like perturbations may be useful to validate limit cycle amplitudes and domains of attraction. However, exact validation of unstable limit cycles requires more advanced experimental setups (e.g., for control-based continuation [21]).

In the future, the effect of adding torsional damping at the king pin could also be investigated. For the numerical simulations, a more intelligent solver could be created which detects the discontinuities and dynamically reduces the time step if needed. Numerical bifurcation analysis of the non-smooth system is also a future task.

Acknowledgements

The authors thank Csaba Hős, PhD and Máté Antali, PhD for the helpful discussions regarding the dynamics of non-smooth systems.

The research reported in this paper was partly supported by the János Bolyai Research Scholarship of the Hungarian Academy of Sciences. The research carried out at BME has been supported by the National Research, Development and Innovation Office under grant no. NKFI-128422 and under grant no. 2020-1.2.4-TÉT-IPARI-2021-00012, as well as by the NRD Fund (TKP2021, Project no. BME-NVA-02) based on the charter of bolster issued by the NRD Office under the auspices of the Ministry for Innovation and Technology. Supported by the ÚNKP-21-3 New National Excellence Program of the Ministry for Innovation and Technology from the source of the National Research, Development and Innovation Fund.

References

- [1] Pacejka, H. "Tyre and Vehicle Dynamics", Butterworth-Heinemann, 2002. ISBN 0-7506-6918-7
- [2] Stépán, G. "Chaotic motion of wheels", *Vehicle System Dynamics*, 20(6), pp. 341–351, 1991.
<https://doi.org/10.1080/00423119108968994>
- [3] Stépán, G. "Delay, nonlinear oscillations and shimmying wheels", In: Moon, F. C. (ed.) *IUTAM Symposium on New Applications of Nonlinear and Chaotic Dynamics in Mechanics: Proceedings of the IUTAM Symposium held in Ithaca, NY, U.S.A., 27 July–1 August 1997*, Springer, 1999, pp. 373–386. ISBN 978-0-7923-5276-1
https://doi.org/10.1007/978-94-011-5320-1_38
- [4] Takács, D., Orosz, G., Stépán, G. "Delay effects in shimmy dynamics of wheels with stretched string-like tyres", *European Journal of Mechanics - A/Solids*, 28(3), pp. 516–525, 2009.
<https://doi.org/10.1016/j.euromechsol.2008.11.007>
- [5] Takacs, D. "Dynamics of towed wheels – Nonlinear theory and experiments", PhD thesis, Budapest University of Technology and Economics, 2010.
- [6] Takács, D., Stépán, G. "Micro-shimmy of towed structures in experimentally uncharted unstable parameter domain", *Vehicle System Dynamics*, 50(11), pp. 1613–1630, 2012.
<https://doi.org/10.1080/00423114.2012.691522>
- [7] Beregi, S., Takács, D., Stépán, G. "Tyre induced vibrations of the car-trailer system", *Journal of Sound Vibration*, 362, pp. 214–227, 2016.
<https://doi.org/10.1016/j.jsv.2015.09.015>
- [8] Beregi, S., Takacs, D., Gyebroszki, G., Stepan, G. "Theoretical and experimental study on the nonlinear dynamics of wheel-shimmy", *Nonlinear Dynamics*, 98(4), pp. 2581–2593, 2019.
<https://doi.org/10.1007/s11071-019-05225-w>

- [9] Beregi, S., Takacs, D., Stepan, G. "Bifurcation analysis of wheel shimmy with non-smooth effects and time delay in the tyre-ground contact", *Nonlinear Dynamics*, 98(1), pp. 841–858, 2019.
<https://doi.org/10.1007/s11071-019-05123-1>
- [10] Meijaard, J. P., Papadopoulos, J. M., Ruina, A., Schwab, A. L. "Linearized dynamics equations for the balance and steer of a bicycle: a benchmark and review", *Proceedings of the Royal Society A: Mathematical, Physical and Engineering Sciences*, 463(2084), pp. 1955–1982, 2007.
<https://doi.org/10.1098/rspa.2007.1857>
- [11] Sharp, R. S., Evangelou, S., Limebeer, D. J. N. "Advances in the modelling of motorcycle dynamics", *Multibody System Dynamics*, 12(3), pp. 251–283, 2004.
<https://doi.org/10.1023/B:MUBO.0000049195.60868.a2>
- [12] Troger, H., Zeman, K. "A nonlinear analysis of the generic types of loss of stability of the steady state motion of a tractor-semitrailer", *Vehicle System Dynamics*, 13(4), pp. 161–172, 1984.
<https://doi.org/10.1080/00423118408968773>
- [13] Darling, J., Tilley, D., Gao, B. "An experimental investigation of car-trailer high-speed stability", *Proceedings of the Institution of Mechanical Engineers, Part D: Journal of Automobile Engineering*, 223(4), pp. 471–484, 2009.
<https://doi.org/10.1243/09544070jauto981>
- [14] Horvath, Z., Takacs, D. "Analogue models of rocking suitcases and snaking trailers", In: Lacarbonara, W., Balachandran, B., Ma, J., Tenreiro Machado, J. A., Stepan, G. (eds.) *Nonlinear Dynamics of Structures, Systems and Devices: Proceedings of the First International Nonlinear Dynamics Conference (NODYCON 2019)*, Volume I, Springer, 2020, pp. 117–126. ISBN 978-3-030-34712-3
https://doi.org/10.1007/978-3-030-34713-0_12
- [15] Horvath, H. Z., Takacs, D. "Stability and local bifurcation analyses of two-wheeled trailers considering the nonlinear coupling between lateral and vertical motions", *Nonlinear Dynamics*, 107(3), pp. 2115–2132, 2022.
<https://doi.org/10.1007/s11071-021-07120-9>
- [16] Thota, P., Krauskopf, B., Lowenberg, M. "Interaction of torsion and lateral bending in aircraft nose landing gear shimmy", *Nonlinear Dynamics*, 57(3), pp. 455–467, 2009.
<https://doi.org/10.1007/s11071-008-9455-y>
- [17] Qin, W. B., Zhang, Y., Takács, D., Stépán, G., Orosz, G. "Non-holonomic dynamics and control of road vehicles: moving toward automation", [eess.SY], arXiv:2108.02230, Cornell University, Ithaca, NY, USA.
<https://doi.org/10.48550/arXiv.2108.02230>
- [18] Gantmacher, F. "Lectures in Analytical Mechanics", MIR Publishers, Moscow, Russia, 1975.
- [19] Engelborghs, K., Luzyanina, T., Samaey, G. "DDE-BIFTOOL v. 2.00: a Matlab package for bifurcation analysis of delay differential equations", Katholieke Universiteit Leuven, Department of Computer Science, Leuven, Belgium, Rep. TW 330, 2001.
- [20] Guckenheimer, J., Holmes, P. "Nonlinear Oscillations, Dynamical Systems, and Bifurcations of Vector Fields", Springer, 1983. ISBN 978-1-4612-7020-1
<https://doi.org/10.1007/978-1-4612-1140-2>
- [21] Beregi, S., Barton, D. A. W., Rezgui, D., Neild, S. "Using scientific machine learning for experimental bifurcation analysis of dynamic systems", *Mechanical Systems and Signal Processing*, 2022.
<https://doi.org/10.1016/j.ymssp.2022.109649>